

Modelling of membrane swelling-shrinking induced mechanical degradation of the Low-Temperature PEMFC

Akshaykumar N. Desai¹, Surajeet Mohanty², Venkatasailanathan Ramadesigan^{1*}, Suneet Singh¹

¹ Department of Energy Science and Engineering, Indian Institute of Technology Bombay, Mumbai 400076, India

² Fuel Cell Development Division, Vikram Sarabhai Space Centre, ISRO, Thiruvananthapuram 695022, India

(*Corresponding Author: venkatr@iitb.ac.in)

ABSTRACT

Low-temperature proton exchange membrane fuel cells (LT-PEMFCs) have emerged as a clean energy solution in the transportation sector and the backup power generator in the deep space mission. Under aggressive cell operating conditions, the likelihood of mechanical failure in the membrane is high, which eventually generates cracks and pinholes, leading to a gas crossover and catastrophic failure. In this work, a physics-based model of the LT-PEMFC is developed using COMSOL Multiphysics to study the effects of clamping pressure, humidity conditions, and temperatures on cell deformation. The physics-based model is validated with the experiments performed on 32 cm² LT-PEMFC with the hybrid flow configuration at 75 °C and 80% RH. The results show that the membrane under the channel experiences cyclic swelling and shrinking than the rib because of the lower compression and higher humidity, thereby accelerating the degradation. By developing a deeper comprehension of these degradation processes, we aim to enhance the durability of LT-PEMFCs through optimized cell design, and operating conditions.

Keywords: Low-temperature PEMFC, membrane swelling-shrinking, mechanical degradation, COMSOL Multiphysics, Physics-based model

NOMENCLATURE

a_0	active surface area (m ²)
c_p	specific heat (J kg ⁻¹ K ⁻¹)
C	species concentration (mol m ⁻³)
D	binary diffusion coefficient (m ² s ⁻¹)
E	Young's modulus (MPa)
E_{eq}	Equilibrium potential (V)
F	Faraday constant (C mol ⁻¹)
i	exchange current density (A m ⁻²)
j	volumetric current density (A m ⁻³)
K	permeability (m ²)

n	number of electrons
P	pressure (Pa)
P_c	capillary pressure (Pa)
R	universal gas constant (J mol ⁻¹ K ⁻¹)
s	saturation
S	stress (MPa)
T	temperature (K)
u	velocity (m s ⁻¹)
w	mass fraction
x	mole fraction
<i>Greek symbols</i>	
α	transfer coefficient
ϵ_p	porosity
ϵ	strain
η	over-potential (V)
μ	viscosity (Pa s)
ν	Poisson's ratio
ξ	electro-osmotic drag coefficient
ϕ	potential (V)
ρ	density (kg m ⁻³)
σ	conductivity (S m ⁻¹)
ζ	transport coefficient
<i>Subscripts</i>	
eff	effective
eq	equilibrium
f	liquid
g	gas
i	species i
l	electrolyte, proton term
S	solid electrode

1. INTRODUCTION

Low-temperature proton exchange membrane fuel cells (LT-PEMFCs) have emerged as a clean energy solution in the transportation sector and the backup power generator in the deep space mission. However, the premature failure of the cell components remains a major barrier to widespread commercialization. From

the multitude of issues pertaining to fuel cell durability, the current study is mainly focused on the challenges associated with the polymer membrane. Chemical and mechanical degradations are the primary causes of membrane deterioration, often working together to accelerate the process. Under aggressive cell operating conditions, the likelihood of mechanical failure in the membrane is high, which eventually generates cracks and pinholes [1,2].

Cracks, pin-holes and delamination of the polymer membrane are considered as limiting factors for the LT-PEMFC's durability. It leads to a gas crossover and catastrophic failure. Polymer membranes used in the fuel cell experience swelling and shrinking under the hydration and dehydration cycling, respectively. This develops mechanical stress inside the membrane, which is in part responsible for the mechanical failures [3,4]. Many researchers have observed that humidification and thermal cycling play a major role in mechanical stress evolution, which results in crack propagation across the membrane thickness [5,6]. Since the humidification-thermal cycling imposes a spatio-temporal variation in the membrane water content, impacting the membrane response [7,8], it is of utmost importance to gain comprehensive knowledge about the membrane's mechanical behaviour in diverse scenarios. This understanding is pivotal for the development of effective strategies aimed at mitigating these issues within fuel cell operating conditions.

Although several characteristics can be observed from the experiments, a physics-based model of the LT-PEMFC is necessary to analyze the stress evolution inside the membrane due to clamping force and hygro-thermal loading and to identify the potential failure location. In the recent studies by Mehrtash et al. [9,10], a numerical model was developed to analyze the visco-elastoplastic hygro-thermal stresses arising inside the membrane due to clamping force and hygrothermal loading. The linear deformation model was considered for the hygrothermal loading, whereas the elastic perfectly plastic model was considered for the membrane's visco-elastoplastic behaviour. The results show that the membrane under the channel degrades faster than the rib because of the lower compression, higher humidity, and thermal residuals. However, the effects of flow channel configuration and reactant transport inside CL was neglected, leading to erroneous prediction as demonstrated by Um et al. [11]. Similarly, Qiu et al. [1] numerically investigated the stress evolution in the membrane between MEA and GDL frames using 2D finite

element (FE) analysis. A structural mechanics-based 2D FE model was utilized for the stress analysis while neglecting the actual electrochemical reactions. Mehrtash et al. [9] concluded that the clamping force imposes nonuniform compression on GDL and adversely affects the micro-pores, which reduces the cell output.

Several studies have reported the impact of clamping force and humidity-temperature cycling on cell performance [10,12]. However, majority of the studies have only considered the structural mechanics, neglecting other physics like electrochemical reactions, fluid flow, heat transfer and species transport. This type of decoupled approach does not provide real-time stress evolution inside the membrane with the cell operation. Other reported models are either 2D or single channel 3D with simplifications like isothermal operation, simplified reaction kinetics and more [7,9,10]. These models do not provide spatial insights into the stress distribution or deformation of the membrane under various flow configurations.

In this work, a physics-based model of the LT-PEMFC is developed to study the effects of clamping pressure, humidity conditions, operating temperatures and flow configurations on cell deformation. The COMSOL Multiphysics is used to build a 3D, multiphase, non-isothermal, steady-state physics-based model. It is a Multiphysics model that couples different phenomena such as charge transfer, liquid water transport, electrochemical reactions, ionomer water transport, porous media flow, heat generation, transport of reactant species and structural deformation. The physics-based model is validated with the experiments performed on 32 cm² LT-PEMFC with the hybrid flow configuration at 75 °C and 80% RH.

2. MATHEMATICAL MODEL

2.1 Computational domain

Here, the fuel cell has six components namely, bipolar plate (BP), channels, gas diffusion layer (GDL), micro-porous layer (MPL), catalyst layer (CL), and membrane. Multi-serpentine flow configuration is used for the reactant supply on the anode and cathode side of the cell. Fig. 1 shows a full-scale 3D computational domain with the necessary boundary conditions. Multi-serpentine flow configuration is selected for the current study because it facilitates uniform reactant distribution and lower pressure drop as compared to parallel and serpentine flow configurations [8,13]. As can be seen

from Fig. 1, the clamping force is applied on the cathode side of the cell and the other sides are remained fixed.

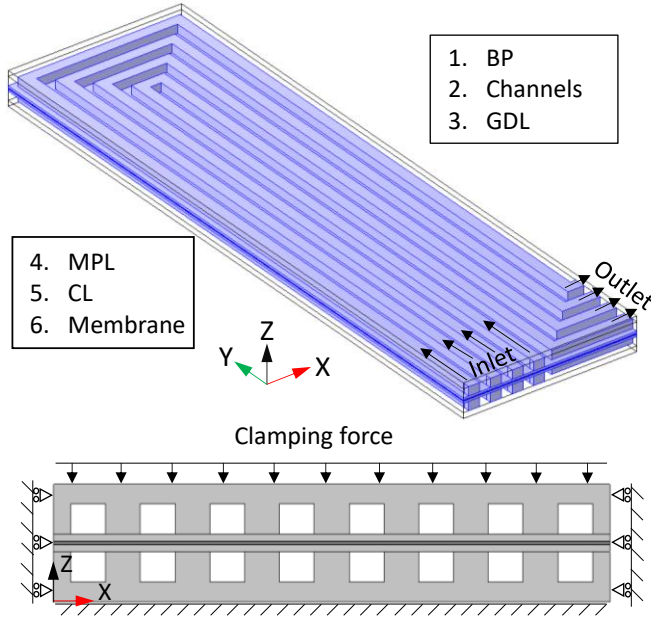


Fig. 1. Computational domain with boundary conditions

The geometrical details of the LT-PEMFC are as follows: height, width and length of a single channel – 0.8, 1, and 55 mm, respectively. The thickness of GDL, MPL, CL and membrane is 0.18, 0.018, 0.01 and 0.045 mm, respectively. The rib width is 0.5 mm. Here only one-fourth of the full domain is considered for the simulation due to computational limitations. A comprehensive 3D, multiphase, non-isothermal, steady-state physics-based model of the LT-PEMFC is developed using the governing equations and empirical correlation from the previous studies. It is solved using a finite element method based COMSOL Multiphysics software. During the simulation, several assumptions are made without losing the general characteristics of the cell.

Assumptions:

- Laminar and incompressible flow due to low velocity
- Cell operation under steady state condition
- Neglected H₂ & O₂ gas cross-over across membrane
- Isotropic and homogeneous material properties
- Effect of gravity on liquid water is neglected
- Linear elastic model considered for the membrane

2.2 Governing equations

Due to space constraints, the main governing equations are only presented here. Other constitutive relations and source terms are available in the literature [14–16]. Porous media flow is modelled using the Brinkman equation and the bulk flow inside the channel is modelled using the Navier-Stokes equation. Reactant transport driven by diffusion and convection is governed by the Maxwell-Stefan diffusion equation. Butler-Volmer kinetics are applied for the hydrogen oxidation reaction and oxygen reduction reaction. Ionic and electronic charge transfer across the cell is governed by Ohm's law. The energy equation is implemented for the heat generation and dissipation across various components of the LT-PEMFC. Water transport across the membrane occurs due to the electro-osmotic drag and back-diffusion, which is evaluated using a flux equation as shown in Table 1.

For the liquid water transport inside the cathode domain, a modified Darcy's law is used including the capillary pressure-saturation gradient. The linear elastic theory is considered for the structural deformation of the components under different loading conditions. The deformation of the body or total strain tensor consists of thermal, elastic and swelling strain components. Swelling strain is only considered in the membrane. Governing equations are shown in Table 1.

Table 1 Governing equations used for the physics-based model

$\nabla \cdot (\rho_g u_g) = S_m$	1
$\frac{\rho_g}{\varepsilon_p} \left((u_g \cdot \nabla) \frac{u_g}{\varepsilon_p} \right) = -\nabla P_g + \nabla \cdot \left[\frac{\mu_g}{\varepsilon_p} (\nabla u_g + (\nabla u_g)^T) - \frac{2\mu_g}{3\varepsilon_p} (\nabla \cdot u_g) I \right] - \frac{S_m}{\varepsilon_p^2} u_g + S_u$	2
$-\nabla \cdot \rho_g w_i \sum_{i=0}^N D_{eff,i} \left[\nabla x_i + \frac{1}{P_g} ((x_i - w_i) \nabla P_g) \right] + \rho_g (u_g \cdot \nabla) w_i = S_i$	3
$j_a = i_{0,a} a_0 \left[\exp \left(\frac{\alpha_a n F \eta}{RT} \right) - \exp \left(\frac{\alpha_a n F \eta}{RT} \right) \right]$	4
$j_c = i_{0,c} a_0 (1 - s) \left(\frac{C_{O_2}}{C_{O_2}^{ref}} \right)^{1/2} \left[\exp \left(\frac{\alpha_c n F \eta}{RT} \right) - \exp \left(\frac{\alpha_c n F \eta}{RT} \right) \right]$	5

$$\eta = \phi_s - \phi_l - E_{eq} \text{ and } \nabla \cdot (-\sigma_s \nabla \phi_s) = S_s \text{ and } \nabla \cdot (-\sigma_l \nabla \phi_l) = S_l \quad 6$$

$$\nabla \cdot (\rho_s c_p u_g T) = \nabla \cdot (k_{eff} \nabla T) + S_T \quad 7$$

$$i = -\sigma_l \nabla \phi_l - \frac{\sigma_l \xi}{F} \nabla \mu_0 \text{ and } N_0 = -\frac{\sigma_l \xi}{F} \nabla \phi_l - \left(\zeta + \frac{\sigma_l \xi^2}{F^2} \right) \nabla \mu_0 \text{ and } \nabla \cdot i = 0 \text{ and } \nabla \cdot N_0 = 0 \quad 8$$

$$\nabla \cdot \left[-\left(\frac{K_f \rho_f}{\mu_f} \right) \left(\frac{\partial P_c}{\partial s} \right) \nabla s \right] = S_w \quad 9$$

$$-\nabla \cdot S = F_v \text{ and } S_{ij} = \frac{E(T,RH)}{(1+\nu)(1-2\nu)} [\nu \delta_{ij} \epsilon_{kk}^{el} + (1-2\nu) \epsilon_{ij}^{el}] \quad 10$$

In this study, Schroeder's paradox is considered in relation to the membrane's behaviour, which manifests distinct water uptake characteristics when exposed to saturated water vapour versus liquid water. When the membrane encounters liquid water, its water uptake capacity (referred to as λ) can reach as high as 22, in contrast to a value of 14 observed with saturated water vapour. Consequently, this variance leads to greater membrane conductivity in the presence of liquid water compared to water vapour.

2.3 Operating parameters and Boundary conditions

The operating parameters and material properties used in developing the multiphase model are given in Table 2. The values are either taken from the experiments performed or the literature.

Table 2 Operating parameters used in the development of LT-PEMFC model [9,12,15]

Parameter		Value
Operating temperature	T	75 [°C]
Operating pressure	P	1.5 [bar]
Relative humidity	RH	80 %
Porosity of GDL, MPL, CL	ϵ_0	0.65, 0.45, 0.45
Ionomer volume fraction	ϵ_l	0.3
Permeability of GDL, MPL, CL	k_{abs}	6.15×10^{-12} , 6.15×10^{-12} , 1×10^{-13} [m ²]
Pore tortuosity	τ	2.5
Electrical conductivity of GDL, MPL, CL	σ_s	1250, 1250, 350 [S m ⁻¹]
Thermal conductivity of GDL, MPL, CL, membrane	k_s	1.6, 0.53, 0.27, 0.3 [W m ⁻¹ K ⁻¹]
Active surface area	a_0	1.3×10^4 [1/m]
Contact angles of GDL, CL	θ	135°, 80°
Evaporation rate constant	k_e	1×10^{-6} [Pa ⁻¹ s ⁻¹]
Condensation rate constant	k_c	100 [s ⁻¹]
Surface tension of water	Υ	0.0696 [N m ⁻¹]

Young's modulus BP, GDL, MPL, CL	E	10, 0.5, 0.5, 0.25 [GPa]
Poisson's ratio	ν	0.25
Exchange current density of anode and cathode	i_0	2.45×10^{-4} , 0.27 [A cm ⁻²]

At the anode and cathode inlet, the temperature, mass flow rate, species mole fraction and liquid water saturation are specified to solve the energy, mass, momentum, species transport and liquid water transport equations. The other transverse boundaries are defined as a no-slip condition. Clamping pressure is applied on the cathode side BP and other boundaries are maintained fixed. The cell is operated under the galvanodynamic conditions. Hygroscopic swelling is only specified for the membrane domain and the thermal expansion is specified for all domains. The detailed boundary conditions used in the current study are mentioned in Table 3.

Table 3 Boundary conditions

Boundary conditions	Value/Correlation
Anode inlet	$\dot{m}_a = 2$ [lpm]
Cathode inlet	$\dot{m}_c = 3$ [lpm]
Anode & cathode outlet	0.5 & 1.5 [bar]
Anode inlet	$1 - \left(\frac{RH \times P_{sat}}{P} \right)$
Cathode inlet	$1 - \left(\frac{RH \times P_{sat}}{P} \right)$
Temperature on BP	75 [°C]
Cathode bipolar plate	I_{cell} [A]
Anode bipolar plate	0 [V]
Clamping pressure on BP	1 & 1.5 [MPa]

3. RESULTS AND DISCUSSION

For the validation purpose, initially, a full-scale LT-PEMFC with a membrane electrode assembly (MEA) area of 32 cm² is simulated without structural deformation. The validation results are shown in upcoming subsection.

3.1 Validation

Experiments are performed on the LT-PEMFC with 32 cm² MEA area at 75 °C and 80% RH. A hybrid flow configuration is used for the reactant supply. Fig. 2 compares the polarization curve of the experiments and a multiphase physics-based model. The multiphase model accounts for the liquid water generation and the resultant impact on the porous domains. Therefore, the results of multiphase model are in good agreement with the experimental results with an RMS current density error of 17 mA/cm². It captures the mass transport limitation identified between 0.6 and 0.4 V cell potentials with reasonable accuracy.

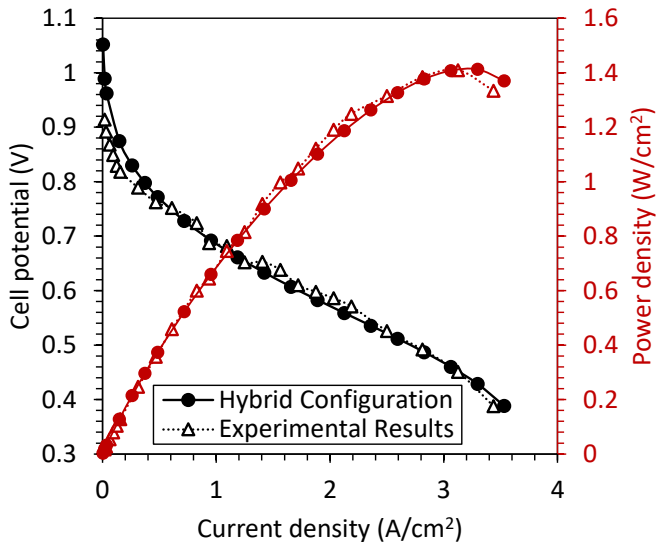


Fig. 2. Comparison between the present physics-based model and the experiments

3.2 Liquid water saturation and temperature

Here, the major objective is to investigate the membrane behaviour under different loading conditions. Therefore, only relevant parameters are presented in this section. As already described, the membrane used in LT-PEMFC has an affinity towards water, which improves its ionic conductivity. At the same time, membrane experiences swelling under humidification and shrinking under dry conditions. This behavior is responsible for generating stresses inside the membrane, which eventually transforms into permanent deformation leading to pinhole or crack propagation. Also, the electrochemical reactions, evaporation/condensation sources and joule heating cause thermal expansion of the membrane. Hence, liquid water saturation and temperature are depicted in Fig. 3.

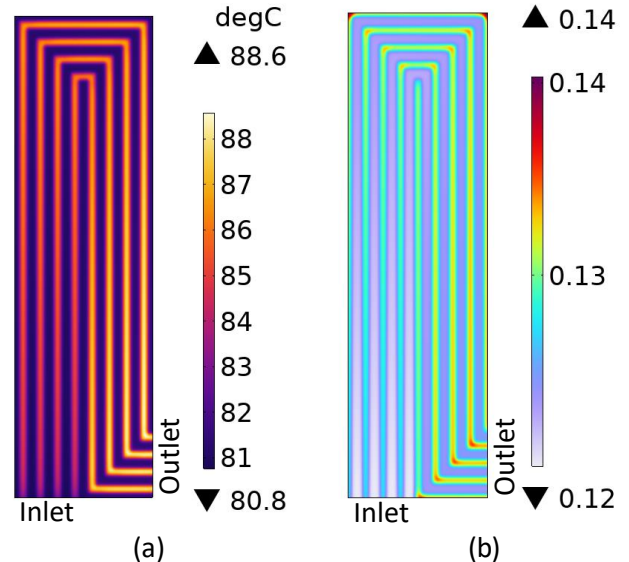


Fig. 3. (a) temperature distribution inside the membrane (b) liquid water saturation on the cathode side at 0.4 V cell potential

To model heat transfer, various heat sources are considered, including joule heating, heat generated by the electrochemical reactions, and the effects of water vapour evaporation and condensation. As the current density increases, the electrochemical reaction intensifies, leading to higher levels of joule heating and the evaporation and condensation of water vapour. Fig. 3 (a) Depicts a temperature variation at the membrane. It is observed that the area under the channel has a higher temperature than rib because of easy reactant supply resulting in rapid electrochemical reactions. This leads to thermal expansion of the membrane under the channel region, which is discussed in upcoming subsections.

The process of condensation and evaporation plays a crucial role in influencing the movement of liquid water within the porous structure of the LT-PEMFC. Fig. 3 (b) illustrates a uniform increase in liquid water saturation in the hybrid configuration, mainly due to uniform reactant distribution and the condensation/evaporation processes. This increase in saturation, from 0.12 at the inlet to 0.14 at the outlet, creates an advantageous pathway for efficient water removal. Consequently, this reduces the risk of water flooding, minimizes mass transport limitations, and enhances the performance of the LT-PEMFC when operating at high current densities. Furthermore, the saturation profile reveals that the rib region contains a higher amount of liquid water than the channel region, which restricts the diffusion of reactants beneath the rib. Higher liquid water under the rib favours

the membrane humidification and maintains its ionic conductivity.

3.3 Effect of clamping force

In this section, the effect of clamping pressure on the membrane electrode assembly (MEA) is studied including the hygroscopic swelling and thermal strains. Applying a compressive/clamping force directly impacts the porosity of diffusion layers. This would be non-uniform across the domain i.e. the regions under the rib will have lower porosity compared to channels due to direct compressive force induced by the ribs. Accordingly, the porosity, permeability and diffusivity of the porous domains are corrected using the volumetric strain.

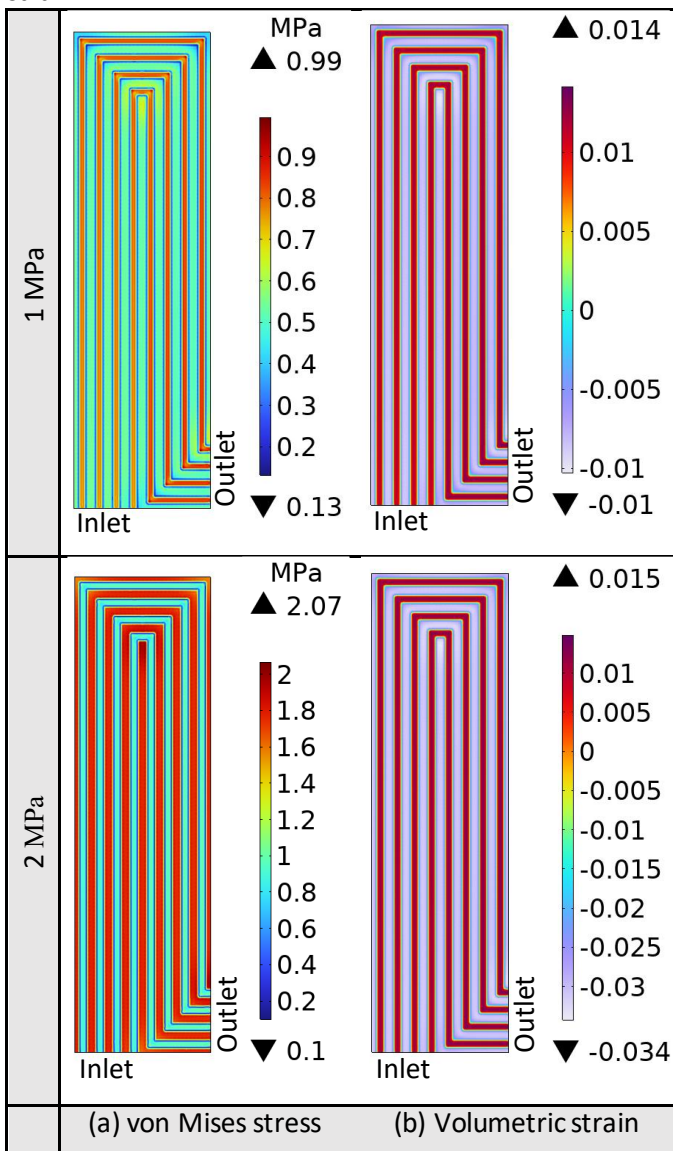


Fig. 4. Membrane behaviour under different clamping pressure (a) von Mises stress (b) volumetric strain

Fig. 4 indicates the variation in von Mises stress and the volumetric strain with changing clamping pressure.

Here, only the membrane domain is considered for the analysis with 1 MPa and 2 MPa clamping forces. It is observed from Fig. 4 (a) that the von Mises stresses are higher under the channel region as compared to the rib region despite of 1 MPa clamping force on the ribs. As discussed earlier, the higher temperature under the channel region induces more thermal strain, leading to higher von Mises stresses. With an increase in clamping force to 2 MPa, it is noticed that the von Mises stresses are higher under the rib regions from Fig. 4 (b). The strain induced with an increase in clamping force and swelling/shrinking surpasses the thermal strain, which causes higher stresses under the rib region. From inlet to outlet, the von Mises stress is increased because of increasing temperature and liquid water saturation.

The volumetric strain is a combination of the thermal strain, swelling/shrinking strain and elastic strain. Here, the positive values of the volumetric strain indicate the expansion and the negative values indicate the compression of the domain. Fig. 4 provides crucial information about the membrane's behaviour under the channel and rib regions. Volumetric strain remains almost same under the channel region for both clamping forces due to thermal strain being a sole contributor. On the other hand, the volumetric (compressive) strain rises from -0.01 to -0.034 with the clamping force. This shows the deformation of the membrane under the rib regions due to direct compressive load. It is seen that the membrane constantly experiences cyclic stresses due to changing liquid water saturation, temperature and clamping pressure, which eventually results in permanent deformation and failure.

The effect of clamping pressure on the various components of the LT-PEMFC can be seen from the deformation profile in Fig. 5. Here, the bottom surface is fixed and top surface is applied with the 1 and 2 MPa of clamping force. Different components like GDL, MPL, CL and membrane experience large compression under the rib compared to channels as expected. It adversely affects the transport properties of the diffusion media like porosity, permeability and diffusivity of the reactants. Diffusion media bulges out/expands under the channel region due to thermal strain and absence of direct load. Fig. 5 (a) shows a maximum deformation of 2.73 μm under 1 MPa clamping force. Here, the combined effects of swelling and thermal expansion cause the membrane deformation. Under 2 MPa clamping force, a maximum deformation of 6.8 μm is observed in Fig. 5 (b).

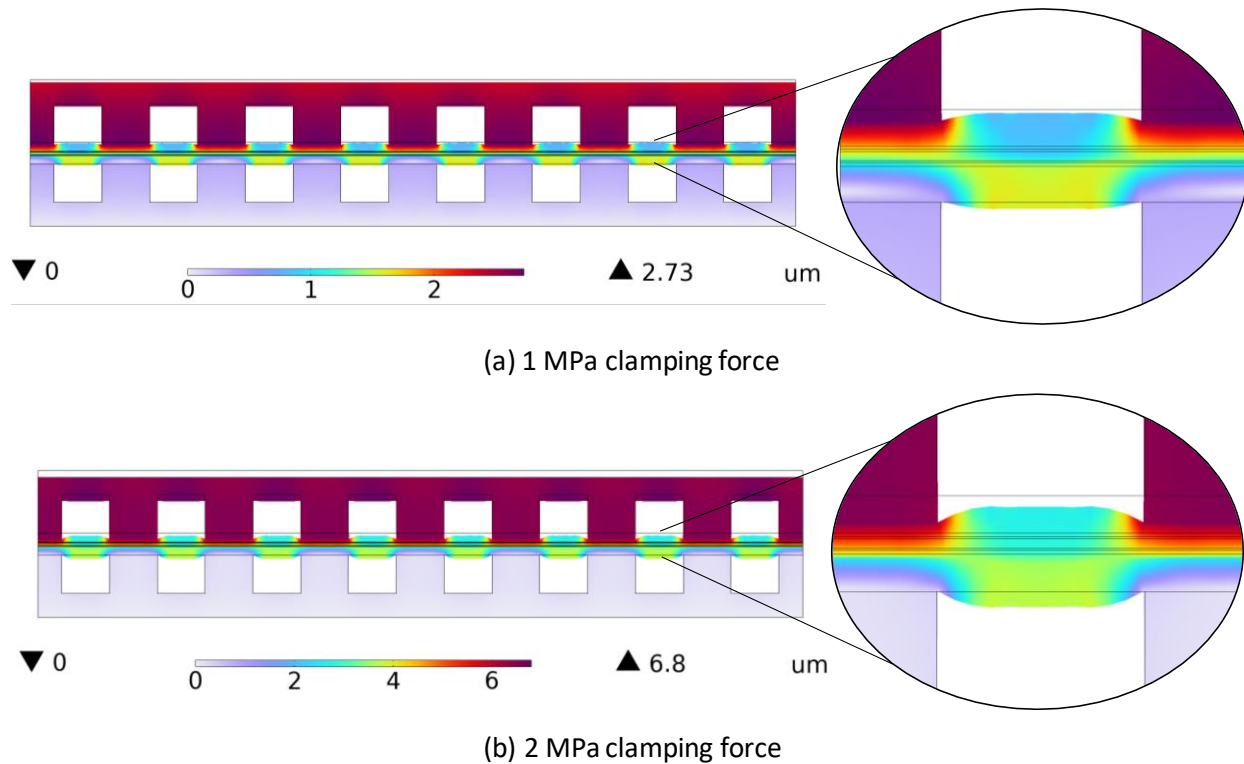


Fig. 5. Deformation of various components of the LT-PEMFC under (a) 1 MPa clamping force (b) 2 MPa clamping force

4. CONCLUSIONS

The present study analyses the effect of clamping force, humidity and temperature on the membrane deformation and other related performance parameters. Using COMSOL Multiphysics, a 3D, non-isothermal, multiphase, steady-state physics-based model is developed to study cell performance. The model consists of electrochemical reactions, species transport, porous media flow, heat generation, liquid water transport, membrane water transport, solid mechanics and charge transfer. It is validated with the experiments and further applied to study the structural integrity.

Increasing saturation from inlet to outlet facilitates easy water removal, maintaining adequate membrane humidification. On the other hand, increasing temperature might cause excessive thermal strain on the membrane, which can be tackled by proper thermal management. It is out of scope for the current work. The results suggest that the membrane under the channel experiences cyclic swelling and shrinking than the rib because of the lower compression and higher thermal expansion, which cumulatively accumulates the stresses and accelerates the degradation. The findings from this work can be used for optimizing the cell design and operating conditions to enhance the membrane's durability. The developed model will help in studying the transient accumulation of the membrane stresses under humidification and thermal cycling.

ACKNOWLEDGEMENT

This work has been funded by the Indian Space Research Organization (ISRO) in collaboration with the Indian Institute of Technology Bombay (IITB) under ISRO-IITB Space Technology Cell grant no. RD/0120-ISROC00-008.

REFERENCE

- [1] Qiu D, Peng L, Liang P, Yi P, Lai X. Mechanical degradation of proton exchange membrane along the MEA frame in proton exchange membrane fuel cells. *Energy* 2018;165:210–22.
- [2] Kusoglu A, Santare MH, Karlsson AM. Aspects of fatigue failure mechanisms in polymer fuel cell membranes. *J Polym Sci Part B Polym Phys* 2011;49:1506–17.
- [3] Lai Y-H, Mittelstadt CK, Gittleman CS, Dillard DA. Viscoelastic Stress Analysis of Constrained Proton Exchange Membranes Under Humidity Cycling. *J Fuel Cell Sci Technol* 2009;6:0210021–02100213.
- [4] Ding G, Santare MH, Karlsson AM, Kusoglu A. Numerical evaluation of crack growth in polymer electrolyte fuel cell membranes based on plastically dissipated energy. *J Power Sources* 2016;316:114–23.
- [5] Kusoglu A, Weber AZ. A Mechanistic Model for Pinhole Growth in Fuel-Cell Membranes during Cyclic Loads. *J Electrochem Soc* 2014;161:E3311–22.

- [6]M.H. Khorasany R, Sadeghi Alavijeh A, Kjeang E, Wang GG, Rajapakse RKND. Mechanical degradation of fuel cell membranes under fatigue fracture tests. *J Power Sources* 2015;274:1208–16.
- [7]Hasan M, Goshtasbi A, Chen J, Santare MH, Ersal T. Model-Based Analysis of PFSA Membrane Mechanical Response to Relative Humidity and Load Cycling in PEM Fuel Cells. *J Electrochem Soc* 2018;165:F3359–72.
- [8]Desai AN, Mohanty S, Ramadesigan V, Singh S. Transient Characteristics of the Low-Temperature PEMFC: A Comparative Analysis Using a Physics-Based Model. 244th ECS Meet., Gothenburg, Sweden: 2023.
- [9]Mehrtash M, Tari I, Yesilyurt S. Impacts of inhomogeneous clamping force on local performance and liquid water formation in polymer electrolyte fuel cells. *Int J Hydrogen Energy* 2017;42:19227–45.
- [10]Mehrtash M, Tari I, Yesilyurt S. Numerical modeling of visco-elasto-plastic hygro-thermal stresses and the effects of operating conditions on the mechanical degradation of PEFC membranes. *J Power Sources* 2018;396:164–74.
- [11]Um S, Wang CY. Three-dimensional analysis of transport and electrochemical reactions in polymer electrolyte fuel cells. *J Power Sources* 2004;125:40–51.
- [12]Kusoglu A, Karlsson AM, Santare MH, Cleghorn S, Johnson WB. Mechanical behavior of fuel cell membranes under humidity cycles and effect of swelling anisotropy on the fatigue stresses. *J Power Sources* 2007;170:345–58.
- [13]Desai AN, Mohanty S, Ramadesigan V, Singh S, Shaneeth M. Simulating the effects of flow configurations on auxiliary power requirement and net power output of High-Temperature Proton Exchange Membrane Fuel Cell. *Energy Convers Manag* 2022;259:115557.
- [14]Weber AZ, Newman J. Transport in Polymer-Electrolyte Membranes II. Mathematical Model. *J Electrochem Soc* 2004;151:A311–25.
- [15]Vetter R, Schumacher JO. Free open reference implementation of a two-phase PEM fuel cell model. *Comput Phys Commun* 2019;234:223–34.
- [16]Rizvandi OB, Yesilyurt S. A pseudo three-dimensional, two-phase, non-isothermal model of proton exchange membrane fuel cell. *Electrochim Acta* 2019;302:180–97.